# R-Matrix calculations for opacities: II. Photoionization and oscillator strengths of iron ion FeXVII, FeXVIII and FeXIX

View the article online for updates and enhancements.

# R-Matrix calculations for opacities: II. Photoionization and oscillator strengths of iron ions Fe XVII, Fe XVIII and Fe XIX

**S N Nahar[1], L Zhao[2], W Eissner[3], A K Pradhan[1]‡**

[1] Department of Astronomy, The Ohio State University, Columbus, Ohio 43210, USA

[2] Department of Physics, The Ohio State University, Columbus, Ohio 43210, USA

[3] Institut für Theoretische Physik, Teilinstitut 1, 70550 Stuttgart, Germany§

E-mail: pradhan.1@osu.edu

**Abstract.** Iron is the dominant heavy element that plays an important role in radiation transport in stellar interiors. Owing to its abundance and large number of bound levels and transitions, iron ions determine the opacity more than any other astrophysically abundant element. A few iron ions constitute the abundance and opacity of iron at the base of the convection zone (BCZ) at the boundary between the solar convection and radiative zones, and are the focus of the present study. Together, Fe XVII, Fe XVIII and Fe XIX contribute 85% of iron ion fractions 20%, 39% and 26% respectively, at the BCZ physical conditions of temperature $T \sim 2.11 \times 10^6$K and electron density $N_e = 3.1 \times 10^{22}$cc. We report heretofore the most extensive R-matrix atomic calculations for these ions for bound-bound and bound-free transitions, the two main processes of radiation absorption. We consider wavefunction expansions with 218 target or core ion fine structure levels of Fe XVIII for Fe XVII, 276 levels of Fe XIX for Fe XVIII, in the Breit-Pauli R-matrix (BPRM) approximation, and 180 LS terms (equivalent to 415 fine structure levels) of Fe XX for Fe XIX calculations. These large target expansions which includes core ion excitations to n=2,3,4 complexes enable accuracy and convergence of photoionization cross sections, as well as inclusion of high lying resonances. The resulting R-matrix datasets include 454 bound levels for Fe XVII, 1,174 levels for Fe XVIII, and 1,626 for Fe XIX up to $n \leq 10$ and l=0 - 9. Corresponding datasets of oscillator strengths for photoabsorption are: 20,951 transitions for Fe XVII, 141,869 for Fe XVIII, and 289,291 for Fe XIX. Photoionization cross sections have obtained for all bound fine structure levels of Fe XVII and Fe XVIII, and for 900 bound LS states of Fe XIX. Selected results demonstrating prominent characteristic features of photoionization are presented, particularly the strong Seaton PEC (photoexcitation-of-core) resonances formed via high-lying core excitations with $\Delta n = 1$ that significantly impact bound-free opacity.

‡ Corresponding author
§ Deceased

*R-Matrix calculations for opacities*                                             2

## 1. Introduction

As described in the first paper in this series *R-Matrix calculations for opacities:I* (RMOP1) [1], solar elemental abundances are uncertain which, in turn, are related to the accuracy of atomic opacities in stellar interiors. Opacity, which is measure of radiation absorption during its transport, is determined by two main processes, absorption by photo-excitations and photoionization via all bound states for all ionization stages of all elements that exist in the plasma, and hence requires extensive amount of atomic data. The present work focuses on high precision atomic data for these two radiative processes. Opacity also depends by photon-electron scattering and free-free transitions, but their contributions are generally small in most of the frequency range at high temperatures and densities.

This work is an extension of the Opacity Project (hereafter OP [2]) which reported findings under the series of *Atomic data for opacities calculations* (ADOC) papers. We first describe the approximations employed in the OP and other prior works and their limitations, and extensions and improvements in the present series.

### 1.1. Atomic data calculations for opacities

Other methods besides the R-matrix method used for large-scale calculations of atomic data for opacities are based on atomic structure calculations for the bound-bound transitions and the distorted wave (DW) approximation for photoionization. Under such approximations, oscillator strengths and photoionization cross sections are computed for all possible bound-bound and bound-free transitions among levels specified by electronic configurations included in atomic calculations.

The DW approximation based on an atomic structure calculation couples to the continuum and yields complete and readily computable datasets for opacities. However, since the DW approximation includes only the coupling between initial and final states, it is unable to produce autoionizing (AI) resonances embeded in the continua formed from the complex interference between the bound and continuum wavefunction expansions involving other levels. DW models employ the independent resonance approximation that treats the bound-bound transition probability independently from coupling to the continuum. In this paper, we report developments in the R-matrix calculations with new features that impact the opacity in contrast to the original OP R-matrix works.

### 1.2. Opacity Project R-matrix calculations

In contrast to atomic structure and DW calculations, the R-matrix method accounts inherently for coupling effects due to electron-electron correlation and introduce autoionizing resonance profiles in an *ab initio* manner. However, R-matrix calculations are computationally laborious and entail multiple steps. The OP work by M.J. Seaton and collaborators [3, 4] was devoted to the development of the R-matrix method using the close coupling (CC) approximation based on implementation framework by

*R-Matrix calculations for opacities*　　　　　　　　　　　　　　　　3

P.G. Burke and collaborators (e.g. [5, 6, 7]). The R-matrix method was employed extensively for accurate calculations of radiative data for energies, oscillator strengths and photoionization cross sections systematically for most astrophysically abundant atoms and ions from hydrogen to iron [2]. The objective of the OP was to determine the stellar plasma opacity using high accuracy radiative atomic data. The atomic data under the OP are available through OP database, TOPbase [8] and NORAD-Atomic-Data [9].

Despite unprecedented effort and advances the OP data are not of sufficient precision or extent, as revealed with the advent of sophisticated high resolution observational and experimental set-ups. The original atomic data from the OP for oscillator strengths ($f$-values) and photoionization cross sections ($\sigma_{PI}$) were found to be inadequate and of insufficient accuracy, primarily because those data were computed in LS coupling without relativistic fine structure effects and with very limited configuration interaction. While OP data included highly excited states with $n \leq 10$, the typical angular momentum limit was $l \leq 3$. Many of these calculations were later repeated for more complete data for $l \leq 9$ using larger wavefunction expansions, and using the BPRM method (these data are available from the NORAD-Atomic-Data database [9]). The main problem for discrepancies was found to be the missing physics manifest at high energies. The OP R-matrix work reported in the ADOC series used small CC wavefunction expansion which included a few LS terms of the ground configuration, or a few configurations of the same n-complex of the target or the core ion. Such considerations missed important physical effects of Seaton PEC resonances first introduced in [10], and Rydberg series resonances corresponding to highly excited core states (demonstrated extensively for oxygen ions [11] and subsequent works). In addition, with high resolution observations fine structure data were needed in contrast to the OP LS coupling data.

### 1.3. Breit-Pauli R-matrix method

The dynamic package of R-matrix codes has been revised and expanded several times. In the follow-up to OP, the Iron Project [12], the R-matrix package was extended to include fine structure with relativistic effects in the Breit-Pauli approximation (the BPRM method [13]). Other physical effects such as radiation damping of AI resonances were also incorporated [14, 15]. Of particular relevance to this work is one of the latest calculations on the convergence of resonant core ion excitations with increasing $n$ for Fe XVII [16].

## 2. Theoretical framework

The BPRM framework is described with particular emphasis on atomic absorption of radiation in plasma sources.

### 2.1. Radiative processes for opacities

The two main processes are photo-excitation for a bound-bound transition and photo-ionization for a bound-free transition. Photo-excitation of an ion $X^+$,

$$h\nu + X^+ \to X^{+*}, \tag{1}$$

is related to oscillator strength (or $f$-value) which gives the probability of transition. Photoionization can occur directly as

$$h\nu + X^+ \to e + X^{++}, \tag{2}$$

which is described by a smooth background cross section or through an intermediate AI state as

$$h\nu + X^+ \leftrightarrow (X^+)^{**} \leftrightarrow e + X^{++} \tag{3}$$

which introduces a resonance in the cross section. A doubly excited AI state is formed when the photon energy matches that of a Rydberg level, $E_R = E_c^* - z^2/\nu^2$ where $E_c^*$ is an excited energy of the core ion, $z$ is the ion charge and $\nu$ is the effective quantum number with respect to $E_c^*$. The state may autoionize into the continuum, or undergo dielectronic recombination if a free electron is captured by emission of a photon via radiative decay of the core ion. The AI resonance can be produced theoretically by including the core excitations in the wave function expansion in the close coupling (CC) approximation.

As mentioned above, opacity can also be caused by scattering of photons by atoms at all frequencies of radiation prevalent in a given environment. However, they are much less significant compared to bound-bound and bound-free transitions and can be taken care more easily as described in the first paper of the series RMOP1.

### 2.2. Close coupling approximation and the R-matrix method

The CC approximation describes the atomic system of (N+1) electrons by a 'target' or the 'core' or the residual ion of N-electrons interacting with the (N+1)th electron. The total wave function, $\Psi_E$, of the (N+1) electrons system in a symmetry $SL\pi$ is represented by an expansion as (e.g. [3])

$$\Psi_E(e + ion) = A \sum_i \chi_i(ion)\theta_i + \sum_j c_j \Phi_j, \tag{4}$$

where the target ion eigenfunction $\chi_i$ is coupled with the $(N+1)^{th}$ electron function $\theta_i$ in a bound or continuum state. The summation is over the ground and as many excited ion states as practical in the CC calculation. $A$ is the anti-symmetrization operator. The $(N+1)^{th}$ electron with kinetic energy $k_i^2$ corresponds to a channel labeled as $S_iL_i\pi_ik_i^2\ell_i(SL\pi)$, where $S_iL_i\pi_i$ is the symmetry of the target state $i$. For $k_i^2 < 0$ the channel is closed and the $\Psi_E$ represents a bound state (all channels closed), and for $k_i^2 > 0$ the channel is open and $\Psi_E$ represents a continuum state. In the second sum, the $\Phi_j$s are bound channel functions of the (N+1)-electron system that account for short-range electron correlation, and subject to an orthogonality condition between

the continuum and the bound electron spin-orbital functions. Autoionizing resonances arise from interference effects among th closed and open channels including core ion excitations in the CC wave function expansion.

In the BPRM method [12, 17] relativistic effects are included in the Breit-Pauli approximation where the Hamiltonian of the (N+1)-electron system is

$$H_{N+1}^{\mathrm{BP}} = \sum_{i=1}^{N+1}\left\{-\nabla_i^2 - \frac{2Z}{r_i} + \sum_{j>i}^{N+1}\frac{2}{r_{ij}}\right\} + H_{N+1}^{\mathrm{mass}} + H_{N+1}^{\mathrm{Dar}} + H_{N+1}^{\mathrm{so}} \tag{5}$$

The curly bracketed term is the non-relativistic Hamiltonian and the additional terms are the relativistic one-body correction terms, the mass correction, $H^{\mathrm{mass}} = -\frac{\alpha^2}{4}\sum_i p_i^4$, Darwin, $H^{\mathrm{Dar}} = \frac{Z\alpha^2}{4}\sum_i \nabla^2(\frac{1}{r_i})$, and the spin-orbit interaction, $H^{\mathrm{so}} = Z\alpha^2\sum_i \frac{1}{r_i^3}\mathbf{l_i}.\mathbf{s_i}$ where $p_i$ is the momentum of an electron, $\alpha$ is the fine structure constant, and $\mathbf{l_i}, \mathbf{s_i}$ are the orbital and spin angular momenta.

Substitution of the CC wavefunction $\Psi_E(e + ion)$ in the Schrodinger equation

$$H_{N+1}\Psi_E = E\Psi_E \tag{6}$$

results in a set of coupled equations that are solved using the R-matrix method [7, 3, 13, 17]. The BPRM method implements an intermediate coupling scheme. The set of $SL\pi$ terms is recoupled for $SLJ\pi$ fine structure levels of the (e + ion) system, followed by diagonalization of the (N+1)-electron BP Hamiltonian. The solutions are either a continuum wavefunction $\Psi_F$ for an electron with positive energies (E $\geq$ 0), or a bound state wavefunction $\Psi_B$ for negative total energies (E < 0).

### 2.3. R-matrix method for radiative data

With wavefunction expansions in the R-matrix formulation as above, transition matrix element for a radiative transition to an excited bound state or for photoionization to a continuum state is given by (e.g. [17])

$$< \Psi_j||\mathbf{D}||\Psi_k >, \tag{7}$$

where the photon-ion interaction is represented by the dipole operator, $\mathbf{D} = \sum_i \mathbf{r}_i$, and the sum is over the number of active electrons.

The generalized line strength $\mathbf{S}$ is expressed as

$$\mathbf{S} = |<\Psi_j||\mathbf{D}_L||\Psi_k>|^2 = \left|\left\langle \psi_f|\sum_{j=1}^{N+1} r_j|\psi_i\right\rangle\right|^2, \tag{8}$$

where $\Psi_j$ and $\Psi_k$ are initial and final state wavefunctions. The line strengths are energy independent quantities. The oscillator strengths ($f_{ij}$) and radiative decay rates or Einstein A-coefficients for E1 dipole transitions are given by

$$f_{ij} = \frac{E_{ji}}{3g_i}S(ij), \quad A_{ji}(a.u.) = \frac{1}{2}\alpha^3\frac{g_i}{g_j}E_{ji}^2 f_{ij}. \tag{9}$$

$E_{ji}$ is the energy difference between initial and final states, and $g_i$, $g_j$ are statistical weight factors of initial and final states respectively.

*R-Matrix calculations for opacities*                                                    6
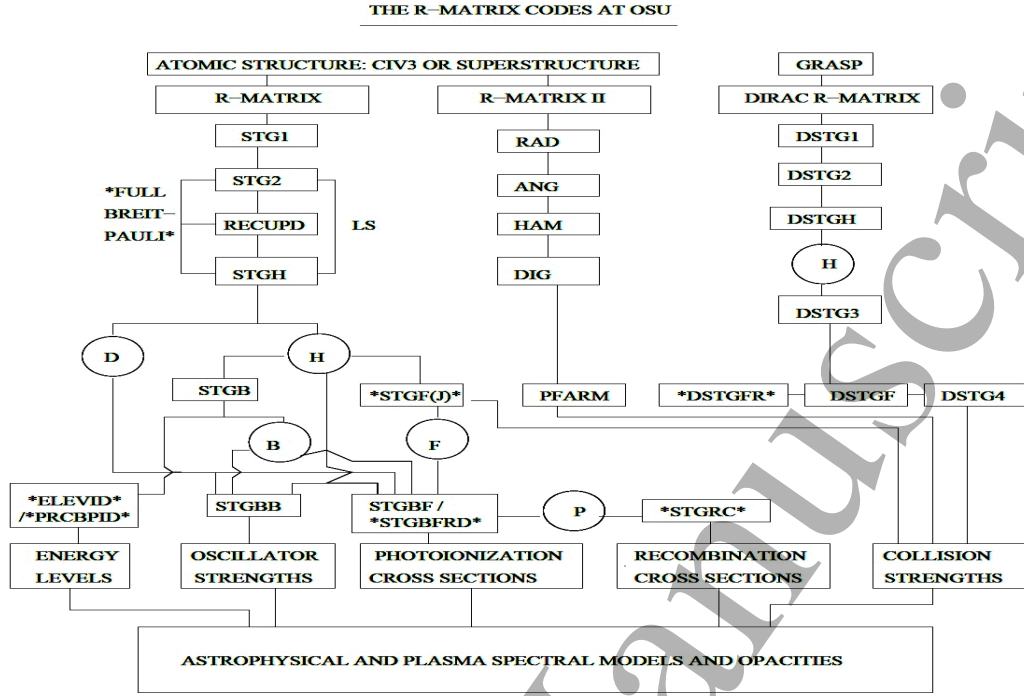


**Figure 1.** Schematic diagram for various stages of R-matrix computations. The data obtained are: 1) energy Levels, 2) oscillator strengths, 3) photoionization cross sections, 4) recombination rate coefficients, and 5) electron impact collision strengths, astrophysical models and opacities calculations.

The photoionization cross section ($\sigma_{PI}$) is obtained as,

$$\sigma_{PI} = \frac{4\pi^2}{3c}\frac{1}{g_i}\omega\mathbf{S},\tag{10}$$

where $g_i$ is the statistical weight factor of the initial bound state and $\omega$ is the incident photon energy. The complex resonant structures in photoionization result from channel couplings between open continuum channels ($k_i^2 \geq 0$) and closed channels ($k_i^2 < 0$) at electron energies $k_i^2$ corresponding to autoionizing states along Rydberg series $S_iL_i\ J_i\pi_i\nu_i\ell_i$, where $\nu_i$ is the effective quantum number relative to the target threshold $S_iL_i\ J_i\pi_i$. We note that present work also includes radiation damping of the resonances using the approach of [14], but is found to be insignificant for the Fe ions considered herein.

## 3. R-matrix Computations for atomic processes

The relativistic R-matrix calculations are carried out through a package of BPRM codes [13, 23, 14] in several stages of computations as shown in Figure 1 (left branch).

BPRM computations begin with the STG1 program for which the program reads the orbital wavefunctions and potentials of the core ion as the first input and computes one- and two-electron radial integrals for the output. In the present cases for Fe XVII,

Fe XVIII and Fe XIX, these wavefunctions are obtained from configuration interaction atomic structure calculations using the code SUPERSTRUCTURE (SS) [18, 19]. The second program STG2 computes spin-angular algebraic coefficients in LS coupling for the ion and (e + ion) Hamiltonian matrices. Program RECUPD recouples the *LS* coefficients in intermediate coupling to introduce fine structure *SLJ*. Using SS wavefunctions, RECUPD also recomputes fine structure energies of the core ion. Typically the energy values and order from RECUPD match closely with those from SS. However, for complex ions they may differ in the third or fourth significant digits and energy order for some levels, particularly those highly excited ones. The program STGH diagonalizes the (e + ion) Hamiltonian to obtain R-matrix basis functions that are used to compute subsequent parameters as follows. Program STGB computes bound energy levels and wavefunctions and STGF computes continuum wavefunctions and electron impact excitation collision strengths. STGBB computes oscillator strengths for bound-found transitions, and STGBF computes photoionization cross sections for bound-free transitions.

### 3.1. Core ion wavefunctions from SUPERSTRUCTURE

As mentioned above, computation using R-matrix codes starts with wavefunctions of the core ion obtained from code SUPERSTRUCTURE (SS). Similar to intermediate coupling in the BPRM method, SS includes relativistic contributions in Breit-Pauli approximation [19]. SS includes several terms of the Breit interaction in addition to one-body terms in BPRM calculations, such as the full Breit interaction and part of other two-body interactions. Configuration interaction calculations are carried out using the Thomas-Fermi-Dirac-Amaldi central potential to compute one-orbitals functions, scaled according to a variational minimization scheme [18, 19, 17].

The list of configurations and Thomas-Fermi orbital scaling parameters for core ions of each of the three Fe ions Fe XVII, Fe XVIII, Fe XIX are given and discussed in following subsections. All configurations for each ion are treated as spectroscopic; that is, all energies are optimized in SS iteratively. Each table quotes the total number of core ion excitation produced by the spectroscopic configurations, all of which were included in wavefunction expansions.

The SS run itself computes a large number of the transitions of types E1, E2, E3, M1, and M2 among all possible levels possible within configurations specified in atomic structure calculations. Although not presented in this paper which focuses on R-matrix results for E1 transitions that primarily contribute to opacities, SS results for all energy levels and all types of transitions stated here are available through atomic database NORAD-Atomic-Data [9].

Progran RECUPD of the R-matrix codes use orbital wavefunctions obtained from SS to recompute the energies of the core ion. These reproduced energies match almost exactly to those from SS for most ions. However, with large complex atomic systems the SS and RECUPD energies can show differences in the third or fourth decimal figures, and

*R-Matrix calculations for opacities*                                                            8

**Table 1.** Optimized set of 17 spectroscopic configurations of the core ion Fe XVIII belonging to complexes n=2,3,4 are: $1s^22s^22p^5(1)$, $1s^22s2p^6(2)$, $1s^22s^22p^43s(3)$, $1s^22s^22p^43p(4)$, $1s^22s^22p^43d(5)$, $1s^22s2p^53s(6)$, $1s^22s2p^53p(7)$, $1s^22s2p^53d(8)$, $1s^22s^22p^44s(9)$, $1s^22s^22p^44p(10)$, $1s^22s^22p^44d(11)$, $1s^22p^63s(12)$, $1s^22p^63p(13)$, $1s^22p^63d(14)$, $1s^22s2p^54s(15)$, $1s^22s2p^54p(16)$, $1s^22s2p^54d(17)$. Thomas-Fermi orbital scaling parameters are: 1.39944(1s), 1.20409(2s), 1.14074(2p), 1.13092(3s), 1.08125(3p), 1.11030(3d), 1.13092(4s), 1.08125(4p), 1.1103(4d). The table present a small sample set of energies from the 218-level set, being compared with those of [20] available at NIST webpage [21]. The number within parentheses next to the LS term corresponds to configuration number for the term.

| i | LS term | 2J+1 | $E_T$(Ry) | E(Ry) | i | LS term | 2J+1 | $E_T$(Ry) | E(Ry) |
|---|---------|------|-----------|-------|---|---------|------|-----------|-------|
| | | | | Total number of levels = 218 | | | | | |
| 1 | $^2P^o(1)$ | 4 | 0.0 | 0.0 | 2 | $^2P^o(1)$ | 2 | 0.94116 | 0.9348 |
| 3 | $^2S^e(2)$ | 2 | 9.8248 | 9.70 | 4 | $^4P^e(3)$ | 6 | 56.798 | 57.70 |
| 5 | $^2P^e(3)$ | 4 | 57.054 | 56.94 | 6 | $^4P^e(3)$ | 2 | 57.502 | 57.50 |
| 7 | $^4P^e(3)$ | 4 | 57.668 | 57.57 | 8 | $^2P^e(3)$ | 2 | 57.906 | 57.80 |
| 9 | $^2D^e(3)$ | 6 | 58.436 | 58.32 | 10 | $^2D^e(3)$ | 4 | 58.471 | 58.36 |
| | | | ... | | | | | | |

also the order of the higher energy levels. In the present work, for both Fe XVII and Fe XVIII, the RECUPD energies are used in the Hamiltonian matrix diagonalization in STGH. Often we replace the core excitation energies by observed energies in order to obtain more accurate positions of resonances with respect to core ion thresholds. However, such replacement may not improve results for the present ions since there are many core levels and overlapping Rydberg series of resonances. Effect of coupling of channels is not affected by slight changes in positions.

*3.1.1. CC wavefunction expansion for* Fe XVII: Table 1 lists the optimized set of 17 configurations with Thomas-Fermi scaling parameters of orbitals that produced the 218 energy evels for the core ion Fe XVIII included in the first summation term on RHS of Eq. (4) to represent the (e + ion) wavefunction expansion for Fe XVII. Table 1 provides only a small sample set of energies $E_T$ of the ground and a few excited levels of Fe XVIII from the full set of 218 levels obtained from SS. SS energies are compared with measured values by [20] available from NIST [21], and found to be in good agreement.

The Hamiltonian matrix for Fe XVII is set up and diagonalized in STGH using these energies and energy order of the core ion reproduced in RECUPD. Partial waves $0 \leq \ell \leq 9$ for the interacting free electron form singlet, triplet, and quintet spins for (e + ion) $LS\pi$ up to L=0-4 of even and odd parities, recoupled in RECUPD to yield total $SLJ\pi$ symmetries with $J \leq 12$. The R-matrix boundary was chosen to be $a_o = 6$ a.u., large enough to ensure all bound orbitals to have decayed to at least $P_{n\ell} < 10^{-3}$.

The second term in RHS of Eq. (4), which represents (e + ion) bound state correlation functions as bound channels in the Hamiltonian, included 42 ($N$+1)-particle configurations with minimum to a maximum number electron occupancies in orbitals

*R-Matrix calculations for opacities*　　　　　　　　　　　　　　　　　　9

**Table 2.** The set of 12 spectroscopic configurations of the core ion Fe XIX (as in table 1), optimized for energies and orbitals with complexes n=2,3,4 in the CC wavefunction expansion of Fe XVIII are: $1s^22s^22p^4(1)$, $1s^22s2p^5(2)$, $1s^22p^6(3)$, $1s^22s^22p^33s(4)$, $1s^22s^22p^33p(5)$, $1s^22s^22p^33d(6)$, $1s^22s^22p^54s(7)$, $1s^22s^22p^34p(8)$, $1s^22s^22p^34d(9)$, $1s^22s2p^43s(10)$, $1s^22s2p^43p(11)$, $1s^22s2p^43d(12)$. The set of Thomas-Fermi scaling parameters for the orbitals are 1.35(1s), 0.9009(2s), 1.12(2p), 1.07(3s), 1.05(3p), 1.10(3d), 1.0(4s), 1.0(4p), 1.0(4d).

| i | LS term | 2J+1 | $E_T$(Ry) | E(Ry) | i | LS term | 2J+1 | $E_T$(Ry) | E(Ry) |
|---|---------|------|-----------|-------|---|---------|------|-----------|-------|
| | | | | Total number of levels = 276 | | | | | |
| 1 | $^3P^e(1)$ | 4 | 0.0 | 0.0 | 2 | $^3P^e(1)$ | 0 | 0.6681 | 0.6857 |
| 3 | $^3P^e(1)$ | 2 | 0.8003 | 0.8150 | 4 | $^1D^e(1)$ | 4 | 1.5675 | 1.5387 |
| 5 | $^1S^e(1)$ | 0 | 2.9543 | 2.9629 | 6 | $^3P^o(2)$ | 4 | 8.4592 | 8.4100 |
| 7 | $^3P^o(2)$ | 2 | 9.0267 | 8.9736 | 8 | $^3P^o(2)$ | 0 | 9.4316 | 9.3862 |
| 9 | $^1P^o(2)$ | 2 | 11.714 | 11.5512 | 10 | $^1S^e(3)$ | 0 | 19.706 | 19.4481 |
| | | | ... | | | | | | |

as given within parentheses: 1s(2-2), 2s(0-2), 2p(3-6), 3s(0-2), 3p(0-2), 3d(0-2), 4s(0-1), 4p(0-1), 4d(0-1). The total angular momenta of Fe XVII selected are J=0-9 of even and odd parities, sufficient for radiative excitations via dipole E1 transitions.

*3.1.2. CC wavefunction expansion for* Fe XVIII: The ground and 275 excited fine structure levels of the core ion Fe XIX included with configuration complexes n=2,3,4, were optimized using a set of 12 configurations given in Table 2 along with the Thomas-Fermi scaling parameters of orbitals, and a small subset of the 276-level expansion for Fe XVIII. The calculated energies from SS are compared with measured values from NIST [21].

The CC expansion for Fe XVIII included $0 \leq \ell \leq 9$ partial waves with doublet, quartet, sextet $LS$ symmetries and $L$=0-4 of even and odd parities of the core ion Fe XIX. The R-matrix basis sets for orbitals contained 20 continuum functions inside the R-matrix boundary of radius 4 $a_o$. The second bound-channel correlation function term in Eq. (4) included 96 ($N+1$)-electron configurations with minimum to a maximum occupancies in orbital as given within parentheses: 1s(2-2), 2s(0-2), 2p(2-6), 3s(0-2), 3p(0-2), 3d(0-2), 4s(0-2), 4p(0-2), 4d(0-1). The total (e + ion) angular momenta $SLJ\pi$ for Fe XVIII was chosen to be $J$=1/2-17/2 of even and odd parities.

*3.1.3. CC wavefunction expansion for* Fe XIX: The atomic data for transition probabilities with fine structure of Fe XIX was computed using BPRM codes. Line and oscillator strengths for bound-bound transitions were computed using an 18CC wavefunction expansion for the core ion Fe XX (details in [28]) since no bound states of Fe XIX are formed with higher core excitations. The computation of photoionization cross sections was initially set with a very large 415CC wavefunction expansion which included n=2,3,4 core ion excitations and resonances up to the high energy region.

*R-Matrix calculations for opacities*    10

**Table 3.** The set of 16 spectroscopic configurations of the core ion Fe XX that was optimized for Fe XIX CC calculations with complexes n=2,3,4 are: $2s^22p^3(1)$, $2s2p^4(2)$, $2p^5(3)$, $2s^22p^23s(4)$, $2s^22p^23p(5)$, $2s^22p^23d(6)$, $2s^22p^24s(7)$, $2s^22p^24p(8)$, $2s^22p^24d(9)$, $2s^22p^24f(10)$, $2s2p^33s(11)$, $2s2p^33p(12)$, $2s2p^33d(13)$, $2s2p^34s(14)$, $2s2p^34p(15)$, $2s2p^34d(16)$ with filled 1s orbital. Thomas-Fermi scaling parameters are: 1.35(1s), 1.25(2s), 1.12(2p), 1.07(3s), 1.05(3p), 1.0(3d), 1.0(4s), 1.0(4p), 1.0(4d), 1.0(4f). A sample set of energies $E_T$ is compared with $E$ [20] available from NIST [21].

| i | LS term | $E_T$(Ry) | E(Ry) | i | LS term | $E_T$(Ry) | E(Ry) |
|---|---------|-----------|-------|---|---------|-----------|-------|
| Total number of levels = 415 and states =180 | | | | | | | |
| 1 | $2s^22p^3(^4S^o)$ | 0.0 | 0.0 | 2 | $2s^22p^3(^2D^o)$ | 1.5091 | 1.4683 |
| 3 | $2s^22p^3(^2P^o)$ | 2.7698 | 2.7549 | 4 | $2s2p^4(^4P)$ | 7.2235 | 7.2029 |
| 5 | $2s2p^4(^2D)$ | 9.6995 | 9.5869 | 6 | $2s2p^4(^2S)$ | 10.9879 | 10.8920 |
| 7 | $2s2p^4(^2P)$ | 11.7840 | 11.6184 | 8 | $2p^5(^2P^o)$ | 18.3096 | 18.1380 |
| 9 | $2s^22p^23s(^4P)$ | 66.4611 | 66.2742 | 10 | $2s^22p^23s(^2P)$ | 66.6114 | |

However, owing to computational limits BPRM computations proved to be impractical. Hence $\sigma_{PI}$ were obtained in the LS coupling approximation. Table 3 lists the optimized set of configurations with Thomas-Fermi scaling parameters of orbitals of Fe XX, and provides a sample set of energies for the ground and a number of excited states, compared with energies from NIST [21]. A large number of odd parity states exist in the high energy region, but they are not allowed for dipole transitions from the ground state $2s^22p^3(^4S^o)$ and therefore corresponding series of strong resonances would not manifest themselves. Hence, a concise set of 56 LS states was chosen which includes all dipole allowed and forbidden transitions from the ground and low-lying states, where the basic physics of transitions with the full set of 415 fine structure levels is retained.

The LS term energies computed in STG2 are in similar order as that of SS but with slight differences in values in the 3rd or 4th figure and a few energies with different order. Partial waves for the Fe XIX calculations included $0 \leq \ell \leq 9$ and formed 89 singlets, triplets, quintets and septets, with the target ion total $L$=0-4 of even and odd parities. The R-matrix basis sets contained 14 continuum wavefunctions, R-matrix boundary was $a_o = 6$ a.u. The bound channel correlation functions included 104 $(N+1)$-particle configurations with a minimum to a maximum number electron occupancies in the orbitals as given within parentheses: 1s(2-2), 2s(0-2), 2p(2-6), 3s(0-2), 3p(0-2), 3d(0-2), 4s(0-1), 4p(0-1), 4d(0-1), 4f(0-1).

## 3.2. Bound states and oscillator strengths

The bound energies were obtained by numerically scanning through eigenvalues of the (e + ion) Hamiltonian with a sufficiently fine energy mesh in effective quantum number, typically 0.001-0.005, and corresponding wavefunctions were computed using program STGB of the R-matrix codes (Figure 1). Comparisons show good agreement between the observed NIST compilation and calculated energies [19, 27, 28]. It may be noted that

the R-matrix calculations encompass a large number of configurations for the (N+1)-electrons atomic system, and generally more accurate and yield more extensive data sets than atomic structure codes such as SS.

The transition parameters, such as, oscillator strengths, line strengths, and radiative decay rates for the iron ions Fe XVII-Fe XIX [19, 27, 28] were obtained using program STGBB of the R-matrix codes which uses the Hamiltonian matrix and dipole transition matrices computed by STGH and bound wavefunctions computed by STGB.

### 3.3. Bound-free photoionization cross sections

Basic physical features and illustrative results from large-scale computations of photoionization cross sections ($\sigma_{PI}$) of the three Fe ions Fe XVII, Fe XVIII and Fe XIX were obtained using the STGBF program of the R-matrix package of codes. The $\sigma_{PI}$ of Fe XVII and Fe XVIII reported herein have been obtained from new BPRM calculations. Whereas the $\sigma_{PI}$ of Fe XIX are taken from [22] but features relevant to opacities calculations are highlighted and discussed for comparison, consistency and completeness.

Owing to large sizes of arrays and matrices, the BPRM codes went through an extensive revisions for opacities calculations. Often the computations could be carried out only for few energy levels and photon energies at a time, and required several years to complete.

Photoionization cross sections are obtained with consideration of radiation damping implemented in BPRM codes [13, 23, 14], although eventually found not to be significant for opacities for these Fe ions. Autoionizing resonances in photoionization span wide energy ranges, and were resolved with variable and appropriately fine energy meshes.

## 4. Results and discussion

Opacity calculations require complete datasets for any and all atomic species. We report more extensive studies of the three Fe ions, Fe XVII, Fe XVIII and Fe XIX, than previous works and which also reveal new features in photoionization not observed before. With the objective of obtaining high accuracy and complete sets of atomic data we calcauted transition probablities and photoionizatio cross sections of levels with $n \leq 10$ and $l \leq 9$, and all associated $SLJ\pi$ spin-orbital symmetries, with large wavefunction expansions that show important features in high energy regions. Selected results and prominent characteristic features are discussed below.

### 4.1. Energy levels and Oscillator strengths

We obtained large sets of fine structure energy levels for the three Fe ions Fe XVII, Fe XVIII and Fe XIX [19, 27, 28]. The number of energy levels and oscillator strengths obtained from BPRM method for each ion are given in Table 4. For calculating oscillator strengths between bound-bound transitions, size of the CC wavefunction expansions was

*R-Matrix calculations for opacities*                                                    12

**Table 4.** The table lists the number of energy levels and oscillator strengths for bound-bound transitions obtained for three iron ions. The numbers are nearly the same as those obtained in earlier works with much smaller wavefunction expansions.

| Ion | No. of energies | No. of oscillator strengths | Reference |
|---|---|---|---|
| Fe XVII | 454 | 20,951 | Nahar et al (2003)[19] |
| Fe XVIII | 1174 | 141,869 | Nahar (2006)[27] |
| Fe XIX | 1626 | 289,291 | Nahar (2011)[28] |

smaller compared to those for photoionizatio cross sections, since very high excited core ion levels do not lead to additional bound levels of the (e + ion) system. However, the larger number of core ion thresholds included herein for photoionization give rise to many more high lying Rydberg series of autoionizing states that can be much stronger than those from the low lying excited states.

### 4.2. Photoionization cross sections

The BPRM method reveals several characteristic features in photoionization that are of importance in opacity calculations. The features can be characterized based on type of states or levels of the particular ion, and can impact opacities differently depending on energy, temperature and density of plasma in a given region. The following subsections focus on these features.

Resonances in photoionization may play a dominant role as they can increase radiation absorption by orders of magnitude. In particular, the present work shows that one of the main reasons for discrepancy in photoabsorption from past studies is the lack of consideration of resonances due to high lying core excitations. The only way to obtain these resonances inherently is through the close coupling approximation from a large wavefunction expansion that includes sufficiently high excitations. Hence, we include many excited levels belonging to n=2, 3 and 4 complexes for the 3 Fe ions to satisfy this convergence criterion (see also RMOP3).

*4.2.1.   Photoionization of ground states* The accuracy of the ground level and associated transitions are obviously important in all applications. However, in a plasma at different temperatures and densities the photoionization cross section $\sigma_{PI}$ of the ground state is not necessarily the most significant one, and in fact may not dominate bound-free opacity [32]. Typically, $\sigma_{PI}$ has a slowly varying background cross section up to the highest threshold energy in the CC expansion, and then decreases with energy. The Rydberg series of resonances are superimposed up on the background. However, it is the $n$ -complex of the core ion ground and low-lying configurations that produce more prominent resonances compared to higher ones, as their magnitudes weaken. Figure 2 presents photoionization cross sections of the ground states of the three ions Fe XVII-XIX from the present work (blue) and from TOPbase [8] (magenta) for Fe XVII and
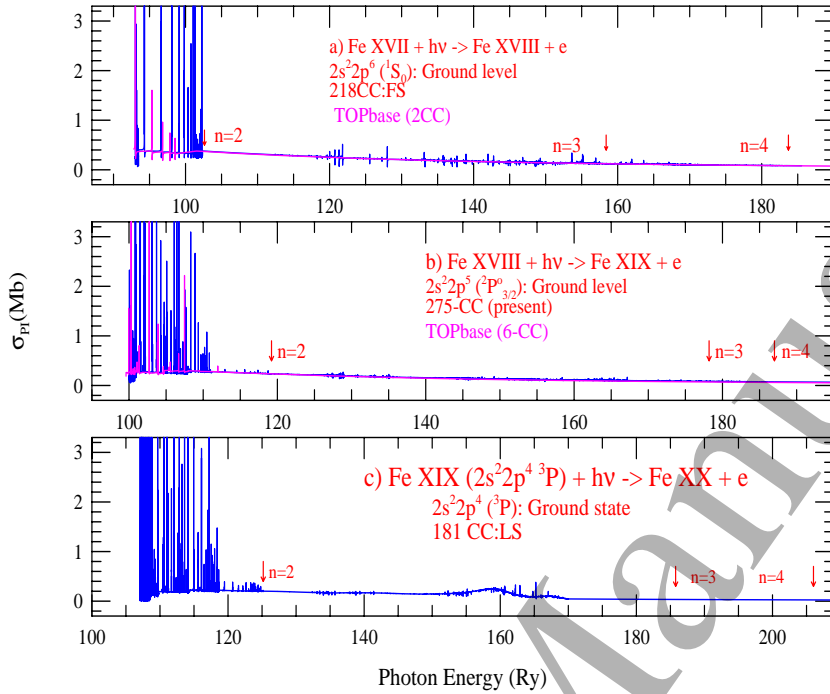
*R-Matrix calculations for opacities*　　　　　　　　　　　　　　　　　13



**Figure 2.** $\sigma_{PI}$ of the ground level of a) Fe XVII (218CC FS), b) Fe XVIII (276CC FS), c) Fe XIX (180CC LS). Present computations with large wavefunction expansion for $\sigma_{PI}$ in blue basically agree with those in magenta from earlier TOPbase calculations with only the ground $n=2$ configuration CC expansion [8]. Hence, photoionization of the ground level is largely unaffected by inclusion of high-level excitations.

Fe XVIII. No other detailed $\sigma_{PI}$ for Fe XIX are found in literature. Our study finds that ground state core excitations beyond $n=2$ complex are not important as they do not produce strong resonances, and inclusion of $n=3$ and 4 levels does not impact cross sections significantly.

*4.2.2.　Relativistic fine structure effect:* In LS coupling resonances in $\sigma_{PI}$ are approximately averaged over their fine structure components. Accuracy increases with inclusion of relativistic fine structure channels as they provide more resolved resonances, more accurate positions of resonances spread over somewhat more extended energy region, as well as additional resonances not allowed in LS coupling. With splitting of LS terms of the core ion states into fine structure levels, a much larger number of excited core ion thresholds is produced, resulting in correspondingly larger number of Rydberg series of resonances. However, the resulting accuracy in $\sigma_{PI}$ may not be significant when the resonances are statistically averaged to obtain integrated quantities such as recombination rates or photoionization rates for plasma opacity at high temperature-

*R-Matrix calculations for opacities*                                                      14

density. But exceptions are noticeable at low energies and in low temperature plasmas when fine structure coupling creates resonant features, which are actually observed in experiments (e.g. [24, 25]), but missing from LS coupling calculations.

Figure 3 demonstrates the effect of coupling of relativistic fine structure channels on photoionization in the near ionization energy for the ground $2s^2 2p^6(^1S_0)$ state of Fe XVII. The upper panel is the present BPRM $\sigma_{PI}$, and the lower panel from a non-relativistic R-matrix calculation in LS coupling [16]. Features in both cross sections are very similar. However, the upper panel shows resonances created by fine structure channels $2s^2 2p^5(^2P^o_{1/2})\epsilon s, d$ in the energy region between the two ground state core ion levels $2s^2 2p^5(^2P^o_{3/2})$ and $2s^2 2p^5(^2P^o_{1/2})$, and an enhancement at the $2s^2 2p^5(^2P^o_{1/2})$ threshold, unlike in coupling without fine structure splitting of $2s^2 2p^5(^2P^o)$. Also, the ionization threshold is lowered to the $2s^2 2p^5(^2P^o_{3/2})$ (pointed arrow), whereas in LS coupling the threshold is at the statistical average of the two levels. These resonances would affect applications in low energy-temperature plasma sources. In addition, it may be noted that fine structure has split the resonances in LS coupling in lower panel into its component resonances in the upper paner. It has been found for the ion that relativistic fine structure effect near the ionization threshold exists in $\sigma_{PI}$ of most of the excited levels of the ion.

*4.2.3. Photoionization of equivalent electron states:* Equivalent electron levels/states, with more than a single electron in the outer orbit, typically have photoionization cross sections with smooth background with some enhancement at core ion thresholds, and then decrease slowly with energy. These levels, particularly the ones formed from excited configurations, produce high-peaked closely-spaced Rydberg series of resonances at lower energies. These resonances typically belong to the core ion excitations of the same $n$-complex as the ground state. Hence these states can have significant impact on applications in relatively low temperature plasmas.

For the present three ions, there is no equivalent electron state for Fe XVII, one for Fe XVIII and three for Fe XIX. Photoionization cross sections ($\sigma_{PI}$) of these levels for Fe XVIII and Fe XIX are shown in Figures 4 and 5. Figure 4 presents $\sigma_{PI}$ of the equivalent electron state $2s2p^6(^2S_{1/2})$ of Fe XVIII. The arrows point to positions of various core ion thresholds where Rydberg series of resonances converge and enhance the background. It may be noted that closely-spaced Rydberg resonances are highly-peaked and strong only for n=2 core ion thresholds. Higher ones are very weak resonances merging with the background.

Figure 5 presents $\sigma_{PI}$ of the three equivalent electron states of Fe XIX: a) $2s2p^5(^3P^o)$, b) $2s2p^5(^1P^o)$, and c) $2p^6(^1S)$. Features are similar to those of Figure 4, with almost no resonance structures beyond $n = 2$ threshold excitations. However, note that $\sigma_{PI}(2s2p^5(^3P^o))$ in panel a) shows closely-spaced strong resonances, those are sparse for the other two levels in panels b) and c). The reason for the latter is lack of the channel couplings with the singlet states $2s2p^5(^1P^o)$ and $2p^6(^1S)$.
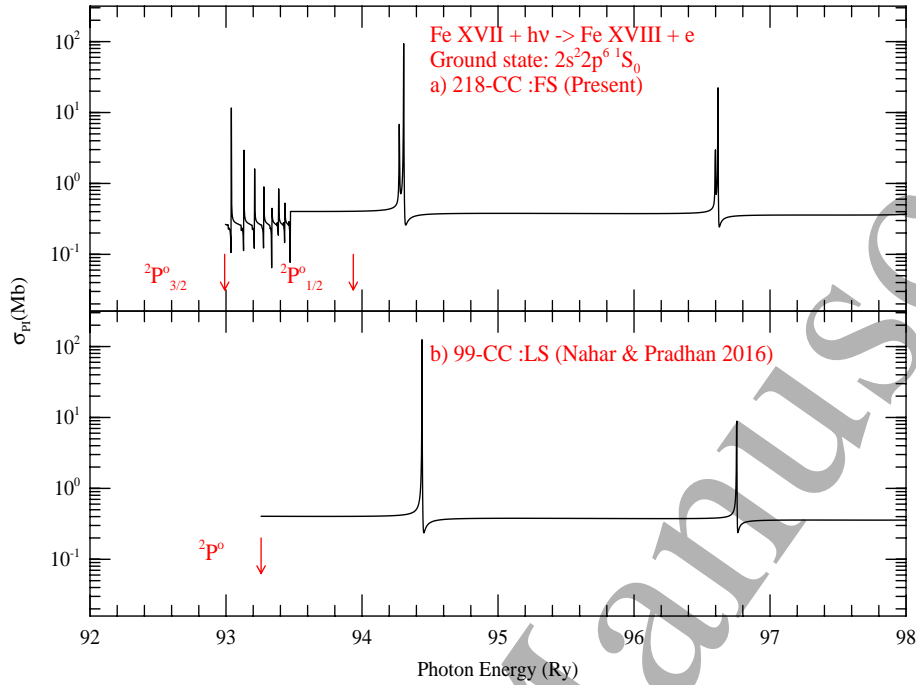
*R-Matrix calculations for opacities*                                                          15



**Figure 3.** Photoionization cross sections $\sigma_{PI}$ in BPRM method of the ground level $2s^2 2p^6(^1S_0)$ of Fe XVII in the near ionization threshold region (upper panel), and non-relativistic LS coupling R-matrix cross sections (lower panel, [16]), showing the coupling effect of fine structure channels in the region between $2s^2 2p^5(^2P^o_{3/2})$ and $2s^2 2p^5(^2P^o_{1/2})$ in the upper panel with resonances and background jump at $2s^2 2p^5(^2P^o_{1/2})$, not formed in LS coupling.

*4.2.4. Photoionization of low-lying excited levels:* Photoionization features change dramatically for single-electron excited states in comparison to those of the ground and equivalent electron states. Core excitations to high lying levels beyond the ground $n$-complex exhibits enriched variations. For the three Fe ions, considerable impact can be seen in $\sigma_I$ of excited states in forming strong resonances and enhancing the background beyond the ground n-complex (n=2), even for the first excited level illustrated in Figure 6.

Figure 6 presents $\sigma_{PI}$ of the first single valence electron excited level $2s^2 2p^5 3s(^3p^o_2)$ of Fe XVII; blue represents this work and black the OP data obtained by M. P. Scott (unpublished) available in TOPbase [8]. Regions of resonant features belonging to core excitation to $n$ =2, $n$ =3 and $n$ =4 complexes are marked by arrows which point to energies of the highest excited core of the respective $n$ -complex; those associated with $n$ =2 are very weak and the background cross section is decreasing. However, above $\sim$ 57 Ry strong resonance structures appear and dominate until $n$ =3 thresholds around $\sim$97 Ry, where the background rises by more than on order of magnitude. Beyond $n$
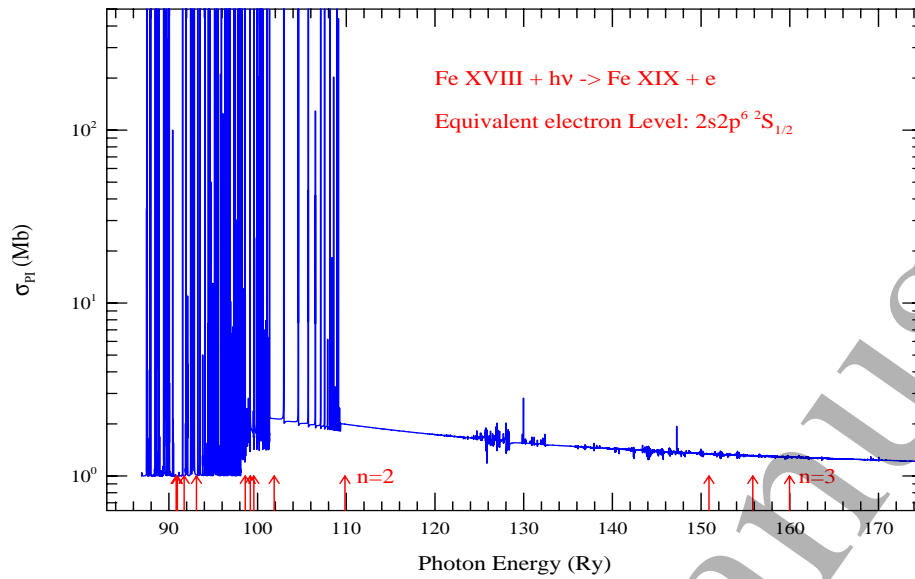
*R-Matrix calculations for opacities* 16



**Figure 4.** $\sigma_{PI}$ of the equivalent electron state $2s2p^6(^2S_{1/2})$ of Fe XVIII. Arrows at the bottom indicate excitation thresholds to which Rydberg series of resonances converge. Arrows at n=2 and n=3 indicate the highest core ion excitation energy for the respective shell. Features show formation of very strong series of $n = 2$ resonances; higher ones are much weaker.

=3, resonances become weak and merge with the smooth background which decreases smoothly. The strength of the $n$ =3 resonance complex, relative to $n$ =2, indicates high photoabsorption and enhanced background missing in OP data [8].

Figure 7 presents $\sigma_{PI}$ of the first single valence electron excited level $2s^22p^43s(^4Po_{5/2})$ of Fe XVIII where the arrows point to the energy positions of the highest excited core of the respective shells $n$ =2,3,4. Although it has one less electron, F-like instead of Ne-like Fe XVII, the features are similar indicating characteristics of the level: large enhancement due to $n$ =3 complex of resonances relative to $n$ =2. Couplings to the $n$ =4 complex are very weak and the background decreases with energy. Overall, between ∼60-102 Ry resonant excitations raise the background by more than an order of magnitude, and merge into the background above the $n$ =3 thresholds.

Figure 8 presents $\sigma_{PI}$ of the first single electron excited state, $2s^22p^33s^3S^o$ of Fe XIX demonstrating relative magnitudes of resonant complexes due to $n$ =2 and $n$ =3 thresholds, However, similar to Fe XVII and Fe XVIII the impact is negligible for $n$ =4 complex. *Therefore, it may be concluded that resonance structures due to core excitations beyond n =4 for all three Fe ions have converged.*

*4.2.5. Seaton PEC resonances:* In addition to dense and strong Rydberg series of resonances, the high lying excited states typically show dominance by huge resonances
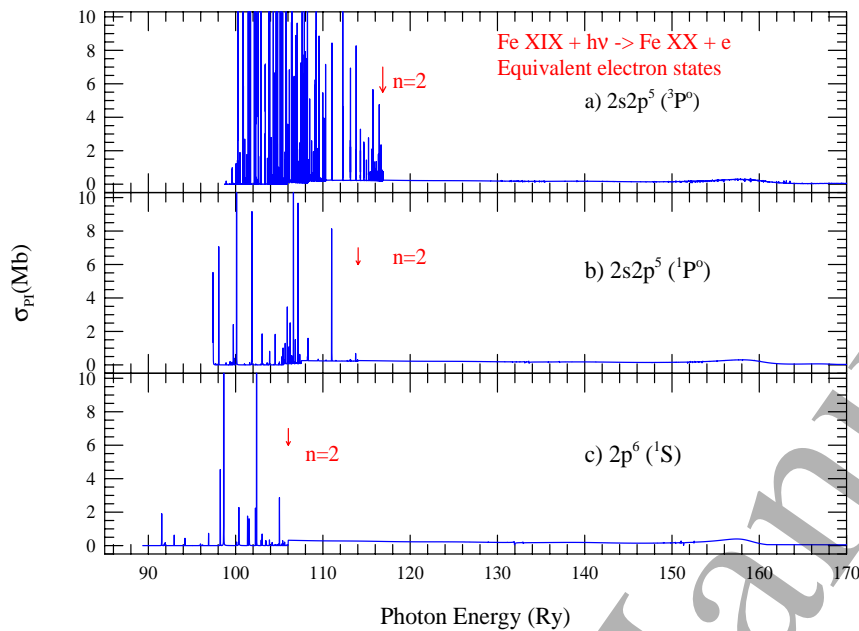
*R-Matrix calculations for opacities* 17



**Figure 5.** $\sigma_{PI}$ of the equivalent electron states a) $2s2p^5(^3P^o)$, b) $2s2p^5(^1P^o)$, and c) $2p^6(^1S)$ of Fe XIX. Arrows at n=2 indicate the highest core ion excitation energy threshold for the shell and appearance of resonances below it. Features show formation of very strong dense series of resonances for $2s2p^5(^3P^o)$ for stronger coupling while it they are less for the singlets due to lack of coupling couplings to the states.
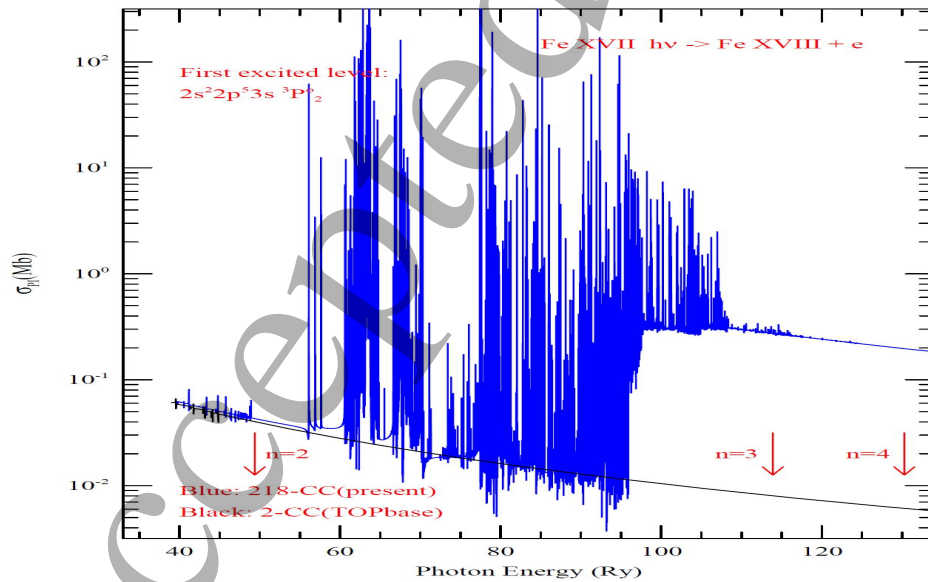


**Figure 6.** $\sigma_{PI}$ of the first single valence electron excited level of $2s^2 2p^5 3s(^3p_2^o)$ of Fe XVII, demonstrating impact of the $n$ =3 complex of resonances forming strong resonance features that are several orders of magnitude higher than those due to the $n$ =2 complex and background enhancement near the $n$ =3 threshold; however, beyond the $n$ =3 resonances are very weak.
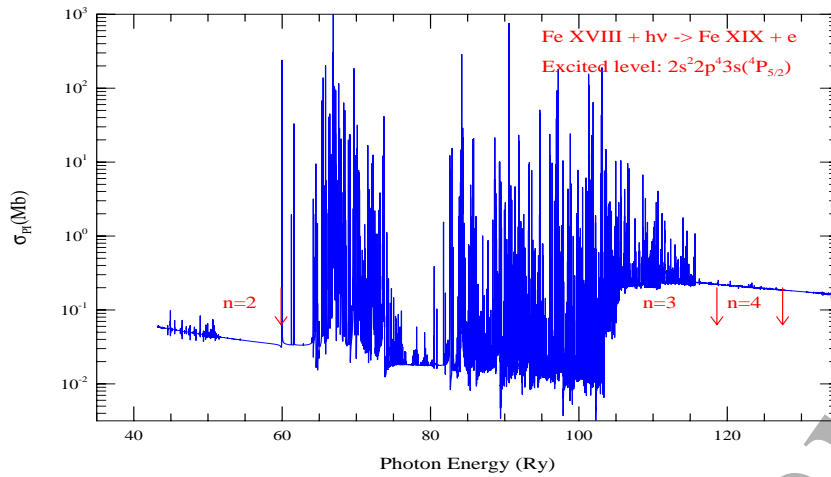
*R-Matrix calculations for opacities* 18



**Figure 7.** $\sigma_{PI}$ of the first single electron excited level $2s^22p4^43s(^4P_{5/2}$ level of Fe XVIII demonstrating core excitations of the $n=3$ complex similar to that of Fe XVII in Figure 6.
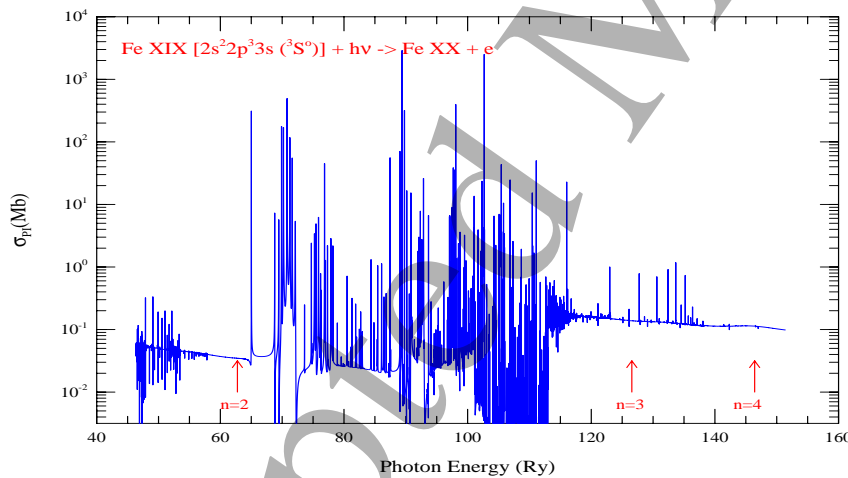


**Figure 8.** $\sigma_{PI}$ of the first excited level of $2s^22p^33s^3S^o$ of Fe XIX, as for Figures 6 and 7.

due to photo-excitation-of core via strong dipole transitions over extended energy regions [10, 17, 26]. Figure 9 presents $\sigma_{PI}$ of the high-lying single valence electron excited level $2s^2p^3(^2D^o)4d(^3S^o)$, of Fe XIX. Generally, Seaton PEC resonances are formed as the core ion is excited from the ground state through a dipole allowed transition, while the outer electron remains a spectator as it photoionizes [33]. The interference of Seaton and Rydberg resonances usually form a combined resonance feature over a wide energy range, as seen around $\sim$70 Ry and $\sim$95 Ry (red arrows) in Figure 9. Since the transition

*R-Matrix calculations for opacities*                                                          19
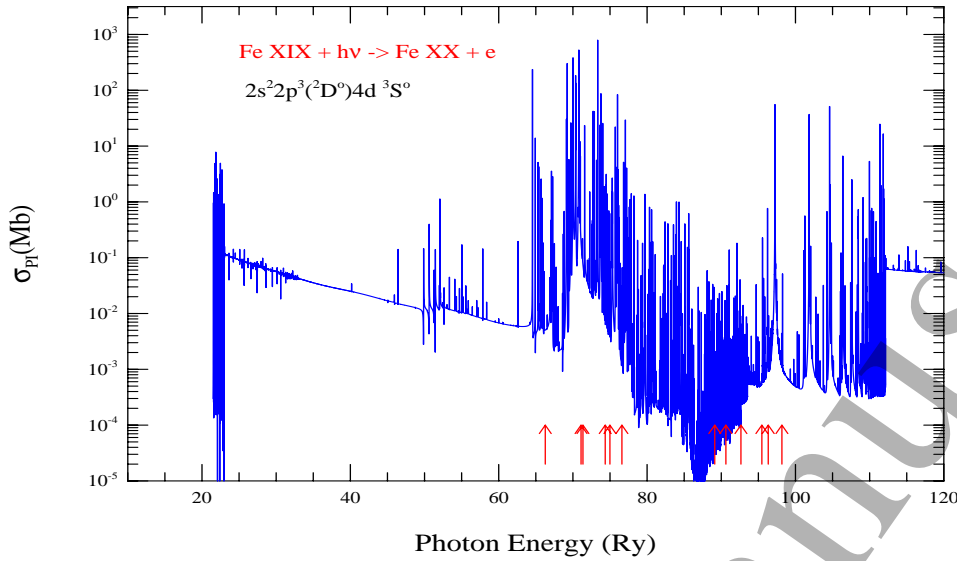


**Figure 9.** Characteristic features of a high-lying excited state, $2s^2p^3(^2D^o)4d(^3S^o)$, of Fe XIX . Photoionization of such levels is typically dominated by wide Seaton PEC resonances, as seen at energy positions pointed by red arrows. Interference of Seaton and Rydberg resonances can impact the background over a wide energy range up to and above 100 eV, and enhancement by more than an order of magnitude above the background.

energies remain the same irrespective of ionization thresholds, Seaton resonances appear at the same photon energies in $\sigma_{PI}$ of all excited levels, but not in $\sigma_{PI}$ of equivalent electron states shown in Figure 5.

Figure 10 illustrates other characteristics of Seaton resonances, the progressive behaviour and commonality in positions at the same PEC energies. Figure 10 shows $\sigma_{PI}$ of three excited levels with different ionization energies: a) $2s^2p^43p(^4D^o_{3/2})$ at $\sim$41 Ry, b) $2s^22p^44f(^2P^o_{1/2})$ at $\sim$19.07 Ry and c) $2s^22p^47f(^2P^o_{1/2})$ at $\sim$5.06 Ry of Fe XVIII. The first two resonances appear around 10 Ry, but seen only for the third excited state (panel c) since the ionization threshold for the level is lower than for these PEC excitations. Other Seaton resonances are at higher energies and appear in $\sigma_{PI}$ of all levels exactly at the same transition energies. The general feature is that Seaton resonances become more prominent with exciation level, from a) to c) in Figure 10. Finally, we also find that Seaton resonances with $\Delta n=1$ are stronger than than those with $\Delta n=0$, but weaker for higher core transition energies $\Delta n$.

Finally, these PEC phenomena should be detectable experimentally owing to their extended energy ranges. By virtue of their immense magnitude and extent, Seaton PEC resonances are the largest contributor to bound-free opacity.
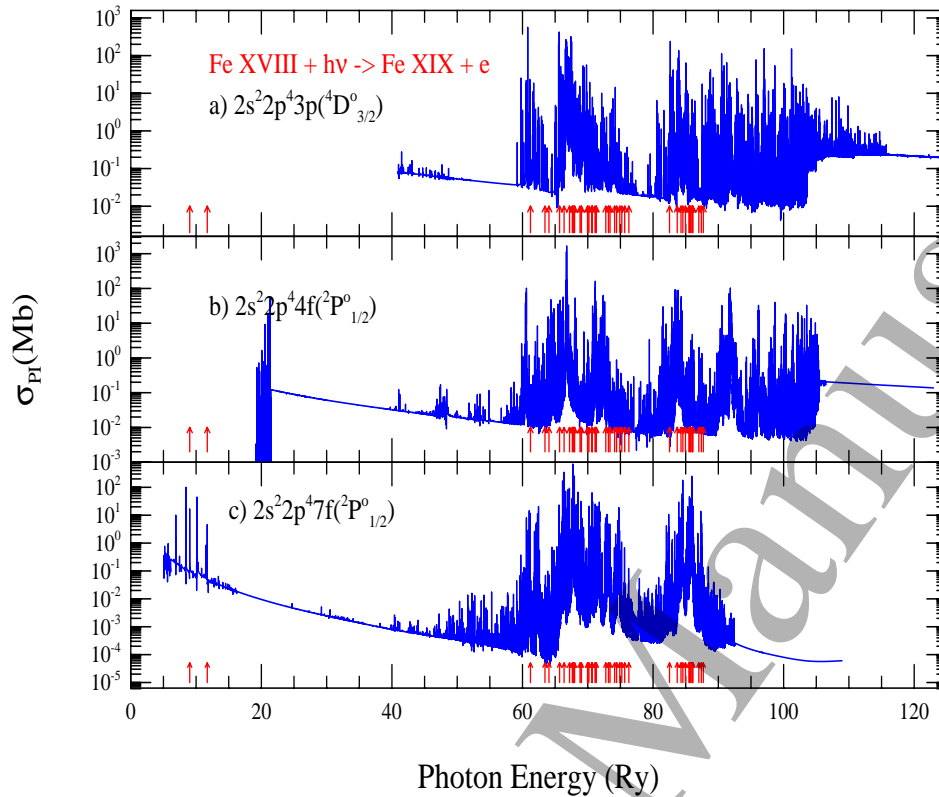
*R-Matrix calculations for opacities*                                    20



**Figure 10.** Progression of chararcterstic features with excitation level: a) $2s^2 2p^4 3p(^4D^o_{3/2})$, b) $2s^2 2p^4 4f(^2P^o_{1/2})$ and c) $2s^2 2p^4 7f(^2P^o_{1/2})$ of Fe XVIII. Seaton resonances appear at the exact energies of core transitions via dipole allowed transitions, and become more prominent in $\sigma_{PI}$ with higher level of $n$ -value of the spectator electron.

*4.2.6. Convergence of resonance series:* One crucial outcome of having a vary large wavefunction expansion which includes many core ion excitations is the convergence of highly-peaked prominent resonant features with increasing principle quantum number n. Exceptions are the $\sigma_{PI}$ of the ground level and equivalent electron levels for which resonances become weaker and start to converge to the background beyond $n = 2$ complex. However, altogether the ground and equivalent electron states are relatively few in number compared to hundreds to over a thousand other excited bound states of each ion where AI resonances dominate. With increasing $n$ , the excitation probability of the core ion first increases and then starts to decrease and weaker channel couplings merging on to the background. In $\sigma_{PI}$ presented in Figures 3-10 for the three Fe ions, we see various progressions with $n = 2$, 3 and 4. The n=4 AI resonance structures are reduced considerably and show the trend towards convergence. Past computations of $\sigma_{PI}$ either did not consider resonances beyond the $n$ -complex of the ground configuration,

*R-Matrix calculations for opacities*                                                                  21

or prominent Rydberg and Seaton resonances and their convergence.

### 4.3. High-energy-density plasmas

The OP and RMOP calculations are carried out for isolated atomic systems that are not markedly perturbed by the plasma environment [34]. Transition probability martix elements are computed using unperturbed bound and continuum wavefunctions in the (e + ion) Hamiltonian with up to thousands of channels for the iron ions considered herein. The R-matrix method accurately accounts for electron correlation effects manifest in the coupling and superposition of channel wavefunctions. The complexity of R-matrix calculations precludes the ideal approach where plasma effects may be directly included in the (e + ion) Hamiltonian in a non-perturbative manner, that may be possible for simpler methods and atomic systems. Whereas the approach in the RMOP work is to adopt the same line broadening treatment for bound-bound transitions as described in OP ADOC papers [2], the effect on extensive autoionizing resonance structures in R-matrix photoionization cross sections are considered perturbatively using a new treatment described in RMOP3. In addition, the inclusion of plasma effects also needs to be consistent with the MHD-EOS formulated for OP assuming unpertubed atomic parameters but introducing an occupation probability factor $w_i$ (RMOP1, Eq. 5).

However, in the high-energy-density (HED) regime the validity of the perturbative approach needs examination. There have been a number of experimental studies on "warm dense matter" created in solid targets irradiated by high-intensity lasers [37, 38], and exotic phenomena such as $K\alpha$ resonance fluorescence [40, 41, 42, 43]. Those are accompanied by DW and atomic structure calculations using non-perturbative methods showing enhancement of photoionization and collisional ionization rates and opacity [39]. The HED plasma effects are more readily incorporated in such models as they are simpler than RMOP calculations and enable more wide ranging studies (viz. [35], SS). In RMOP3 we discuss temperature-density effects in HED plasmas, and demonstrate the effect on photoionization cross sections to ascertain practical limits on densities and other parameters such as Debye screening.

In the OP and RMOP bound-bound and bound-free calculations we include unperturbed energy levels up to $n(SLJ) \leq 10$. But in opacity calculations all levels $10 < n \leq \infty$ must be considered. This high-$n$ contribution to opacity is taken into account by initiating photoionization calculations *below* the first ionization threshold to $E = -z^2/\nu^2$ where $z$ is the ion charge and the effective quantum number $\nu = 10$ (see OP database TOPbase [8, 36]). Since $\sigma_{PI} \sim df/dE$, this additional contribution approximates the oscillator strength due to excitation into $n > 10$ levels [2]. The MHD-EOS truncates $\nu$ further increasingly as function of temperature and density during opacity calculations (Fig. 2, RMOP1).

*R-Matrix calculations for opacities* 22

## 5. Conclusion

We have presented detailed albeit limited sets of photoionization cross sections from extensive calculations for three Fe ions Fe XVII, Fe XVIII  and Fe XIX   that are the dominant iron opacity source in the solar interior at the boundary of the radiative and convection zones (see paper RMOP1). We explore features in the high energy region that include core ion excitations in hundreds of levels of these three ions. These features were not heretofore studied primarily owing to presumption of weak couplings of interacting channels and AI resonance interference effects, as well as practical computational limits. The present study reveals characteristic features of photoionization based on the type of initial bound states and convergence criteria of AI resonant phenomena, and relativistic fine structure effects not produced in LS coupling. Application of these data are expected to provide high-precision plasma opacity in stellar interiors for these ions.

### Data availability statement

All atomic data for energies, radiative transitions, and collisional excitations will be available online at the NORAD-Atomic-Data database at the Ohio State University at: https://norad.astronomy.osu.edu/

### Acknowledgments

*R-Matrix calculations for opacities* 23

## References

[1] Pradhan A K, Nahar S.N. Eissner W (RMOP1) 2024 *J. Phys. B*
[2] The Opacity Project Team .*The Opacity Project*, Vol 1, 1995, Vol. 2, 1996, Institute of Physics Publishing
[3] Seaton M J 1987 *J. Phys. B* 20 6363
[4] Berrington K A, Burke P G, Butler K, Seaton M J, Storey P J, Taylor K T and Yan Y 1987 *J. Phys. B* 20 6379
[5] Burke P G, Robb W D Adv. At. Mol. Phys. 11, 143 (1975)
[6] Burke P G and Taylor K T 1975 *J. Phys. B* 8, 2620
[7] Burke P G 2011 *R-Matrix Theory of Atomic Collisions* Springer
[8] Cunto W, Mendoza C, Ochsenbein F and Zeippen C J 1993 *Astron. Astrophys.* 275 L5 (TOPbase http://cdsweb.u-strasbg.fr/topbase/topbase.html)
[9] Nahar S N 2020 Atoms 8 68 (NORAD https://norad.astronomy.osu.edu/)
[10] Yu Y and Seaton M J 1987 *J. Phys. B* 20 6409
[11] Nahar S N 1998 *Phys. Rev. A* 58 3766
[12] Hummer D G, Berrington K A, Eissner W, Pradhan A K, Saraph H E and Tully J A 1993 *Astron. Astrophys.* 279 298
[13] Berrington K A, Eissner W, Norrington P H 1995 *Comput. Phys. Commun.* 92, 290-420
[14] Zhang H L, Nahar S N, Pradhan A K 1999 *J. Phys. B* 32 1459
[15] The Ohio State group carried out some of the largest computations at the Ohio Supercomputer Center.
[16] Nahar S N and Pradhan A K 2016 *Phys. Rev. Lett.* 116 235003
[17] Pradhan A K and Nahar S N 2011 *Atomic Astrophysics and Spectroscopy* (Cambridge University press, New York)
[18] Eissner W, Jones M, Nussbaumer H 1974 *Comput. Phys. Commun.* 8 270
[19] Nahar S N, Eissner W, Chen G X, Pradhan A K 2003 *Astron. Astrophys.* , 487 789
[20] Sugar J and Corliss C 1985 J. Phys. Chem. Ref. Data 14, Suppl. 2 1
[21] NIST https://physics.nist.gov/PhysRefData/ASD/levels_form.html
[22] Nahar S N 2019 New Ast 73 101277
[23] Nahar S N and Pradhan A K 1994 *J. Phys. B* 27 429
[24] Nahar S N 2002 *Phys. Rev. A* 65 052702
[25] Kjeldsen H, Folkmann F, Hensen J E, Knudsen H, Rasmussen M S, West J B and Andersen T 1999 *Astrophys. J.* 524 L143
[26] Nahar S N 2018 ASP Conf. Ser. 515 93-103
[27] Nahar S N 2006 *Astron. Astrophys.* 457 721
[28] Nahar S N 2011 *Atom. data and Nucl. Data Tables.* 97 403
[29] Computations also faced numerical challenges for complex atomic systems, such as for photoionization of Fe II ([23] the largest calculation at that time), and difficulties with supercomputer systems that also limited the scope of atomic calculations.
[30] Fine structure transitions were obtained from LS multiplets of various ions through algebraic transformation and using observed energies by the National Institute of Standards and Technology (NIST) [21] and Nahar (e.g. [31])
[31] Nahar S N 1995 *Astron. Astrophys.* 293 967
[32] The equation-of-state discussed in RMOP1 determines level populations at a given temperature and density. It is found that only a few percent of total ionic populations may be in the ground state in stellar interiors where thd Fe ions considered herein in are prevalent.
[33] This is the inverse of the dielectronic reombination process when the photoexcited core radiatively decays when a free electron recombines via PEC resonances.
[34] Seaton M J, Yu Y, Mihalas D and Pradhan A K (SYMP) 1994 *Mon. Not. R. astr. Soc.* 266 805
[35] Gu M F 2008, Can. J. Phys., 86, 675
[36] Mendoza C, Seaton M J, Buerger P, Bellorin A, Melendez M, Gonzalez J, Rodriguez L S, Palacios

*R-Matrix calculations for opacities* 24

E, Pradhan A K, Zeippen C J 2007 *Mon. Not. R. astr. Soc.* 378 1031

[37] Vinko S M, Cincosta O, Preston T R, Rackstraw D S and Wark J S 2015, Nat. Commun. 6 6297

[38] Van den Berg Q Y, Fernandez-Tello E V , Burian, T, Chalupsky J, Chung H-K, Ciricosta O, Dakovski G L, Hajkova V, Hollebon P, Juha L *et al.* 2018 *Phys. Rev. Lett.* 120 055002

[39] Zeng J L, Gao C, Liu P F, Li Y J, Meng C S, Hou Y, Kang D D, Yuan J M 2022 China Phys. Mech. Astron. 65, 233011.

[40] Pradhan A K, Nahar S N, Montenegro M, Yu Y, Sur C, Mrozik M *et al.* 2009 J Phys Chem A 113 12356

[41] Vinko S M, Ciricosta O, Cho B I, Engelhorn K, Chung H-K, Brown CRD *et al.* 2012 Nature 482 529;

[42] Cho B I, Engelhorn K, Vinko S M, Chung H-K, Ciricosta O, Rackstraw D S, Falcone R S *et al.* 2012 *Phys. Rev. Lett.* 109 245003

[43] Nahar S N and Pradhan A K 2015 JQSRT 155 32